Upper bound limit analysis of slope stability using rigid finite elements and nonlinear programming

Jian Chen, Jian-Hua Yin, and C.F. Lee

Abstract: In this paper, the development and application of a new upper bound limit method for two- and three-dimensional (2D and 3D) slope stability problems is presented. Rigid finite elements are used to construct a kinematically admissible velocity field. Kinematically admissible velocity discontinuities are permitted to occur at all inter-element boundaries. The proposed method formulates the slope stability problem as an optimization problem based on the upper bound theorem. The objective function for determination of the minimum value of the factor of safety has a number of unknowns that are subject to a set of linear and nonlinear equality constraints as well as linear inequality constraints. The objective function and constrain equations are derived from an energy–work balance equation, the Mohr–Coulomb failure (yield) criterion, an associated flow rule, and a number of boundary conditions. The objective function with constraints leads to a standard nonlinear programming problem, which can be solved by a sequential quadratic algorithm. A computer program has been developed for finding the factor of safety of a slope, which makes the present method simple to implement. Four typical 2D and 3D slope stability problems are selected from the literature and are analysed using the present method. The results of the present limit analysis are compared with those produced by other approaches reported in the literature.

Key words: limit analysis, upper bound, rigid finite element, nonlinear programming, sequential quadratic algorithm, slope stability.

Résumé : Dans cet article, on présente le développement et l'application d'une nouvelle méthode de solution à la limite supérieure de problèmes de stabilité des talus à deux ou trois dimensions (2D et 3D). Des éléments finis rigides sont utilisés pour construire un champ de vélocités cinématiquement admissibles. On permet que des discontinuités de vélocités cinématiquement admissibles se produisent à toutes les frontières entre les éléments. La méthode proposée représente le problème de stabilité de talus comme un problème d'optimisation basé sur le théorème de limite supérieure. La fonction objective pour déterminer la valeur minimale du coefficient de sécurité comprend un certain nombre d'inconnus qui dépendent d'un ensemble de contraintes linéaires et non linéaires d'égalité de même que de contraintes linéaires d'inégalités. La fonction objective et les équations de contraintes sont dérivées d'une équation de balance d'énergie–travail, du critère de rupture (à la limite élastique) de Mohr–Coulomb, d'une loi associée d'écoulement, et d'un certain nombre de conditions aux frontières. La fonction objective avec les contraintes conduisent à un problème standard de progammation non linéaire qui peut être résolu par un algorithme quadratique séquentiel. On a développé un programme d'ordinateur qui rend la présente méthode simple à mettre en application pour trouver le coefficient de sécurité d'un talus. On a choisi dans la littérature et analysé avec la présente méthode quatre problèmes typiques de stabilité de talus 2D et 3D. Les résultats de la présente analyse sont comparés avec ceux obtenus par d'autres approches tels que rapportés dans la littérature.

Mots clés : analyse limite, limite supérieure, élément fini rigide, programmation non linéaire, algorithme quadratique séquentiel, stabilité des talus.

[Traduit par la Rédaction]

Introduction

Slope stability problems are commonly encountered on geotechnical engineering projects. The assessment of slope stability has received wide attention across geotechnical communities because of its practical importance. Numerous analysis methods have been proposed. In general, these methods can be classified into the following three types.

(1) *The limit equilibrium approach:* The methods based on this approach have gained wide acceptance in practice because of their relative simplicity and the experiences accumulated to date. Most of the methods are based on discretization into either vertical slices (e.g., Bishop 1955; Morgenstern and Price 1965; Janbu 1973) or inclined slices (e.g., Sarma 1979; Hoek 1987). With the limit equilibrium method, a failure surface is generally assumed, and the soil mass above the failure surface is then divided into a number of slices. Global static equilibrium conditions for various

Received 2 May 2002. Accepted 19 March 2003. Published on the NRC Research Press Web site at http://cgj.nrc.ca on 18 July 2003.

J. Chen and J.-H. Yin[1]. The Department of Civil and Structural Engineering, The Hong Kong Polytechnic University, Hung Hom, Kowloon, Hong Kong, China. **C.F. Lee.** The Department of Civil Engineering, The University of Hong Kong, Hong Kong, China.

[1]Corresponding author (e-mail: cejhyin@polyu.edu.hk).

 doi: 10.1139/T03-032

assumed failure surfaces are examined, and the critical slip surface corresponding to the lowest factor of safety is sought. While the limit equilibrium methods have been subject to continuous refinement, there is an inherent limitation with these methods in that they are based on assumptions made on the interslice forces to make the problem statically determinate. The methods are hence not rigorous as a result of the use of such assumptions, and it is difficult to assess the accuracy of the solutions.

(2) *Numerical solutions based on continuum mechanics:* With this approach, numerical solutions are obtained based on continuum mechanics. Examples of such methods include (*a*) the finite element method (e.g., Griffths and Lane 1999), (*b*) the discontinuous deformation analysis (e.g., MacLaughlin et al. 2001), and (*c*) the rigid body–spring element method (RBSM or RFEM) (Zhang et al. 2001). These methods can be used to calculate deformations under loading or the factor of safety by iteration. An appropriate constitutive model for the soil mass in the slope is needed with these methods. Using these methods, both the soil movement and progressive failure can be modelled. This allows a better understanding of the mechanisms of failure, especially for the case of progress failure. However, the calculation of the factor of safety needs an iterative or trial-and-error approach. The computing time for solving a stability problem is much larger than that using the limit equilibrium methods. The convergence of computation is another concern. Therefore, these methods have not been widely used for general slope stability analyses in practice.

(3) *Limit analysis approach based on plasticity limit theorems:* Applications of plasticity limit theorems in soil mechanics were first reported in Drucker and Prager (1952) and were further surveyed by Chen (1975). With this approach, a limit analysis takes advantage of the lower and upper bound theorems of classical plasticity to bracket the true solution from a lower bound to an upper bound. These solutions are rigorous in the sense that the stress field with a lower bound solution is in equilibrium with the imposed loads at every point in the soil mass, while the velocity field associated with an upper bound solution is compatible with the imposed displacements. Yu et al. (1998) pointed out that an upper bound limit analysis solution might be regarded as a special limit equilibrium solution but not vice versa.

In recent years, many efforts have been made in the application of the plasticity limit theorems to limit analysis of slope stability. Donald and Chen (1997) proposed an energy–work balance approach (or the upper bound approach using the associated flow rule). Wang et al. (2001) developed this method to investigate the influence of a nonassociated flow rule on the calculation of the factor of safety (FOS) of two-dimensional (2D) soil slopes. Chen et al. (2001*a*, 2001*b*) recently extended the upper bound method for three-dimensional (3D) slope stability analysis. Sloan (1988, 1989), Sloan and Kleeman (1995), and Lyamin and Sloan (2002) have made significant progress in developing new methods using finite elements and linear programming (LP) or nonlinear programming (NLP) for computing rigorous lower and upper bounds for 2D and 3D stability (mainly bearing capacity) problems. The numerical implementation of the limit theorems is based on a finite element discretization of the rigid plastic continuum. This results in a standard linear or nonlinear optimization problem with a highly sparse set of constraints. Using these algorithms, Kim et al. (1999) presented a formulation in terms of effective stresses for performing lower and upper bound limit analysis of soil slopes subjected to pore-water pressures under plain–strain condition.

Recently, Zhang (1999) presented a lower bound limit analysis in conjunction with the rigid finite element method (RFEM) to assess the stability of slopes. The RFEM, which was first proposed by Kawai (1978), has been modified by other researchers (Zhang and Qian 1993; Qian and Zhang 1995; Zhang et al. 1997). The RFEM provides an effective approach to the numerical simulation of the behaviour of discontinuous media. Further studies and applications of the RFEM are still being made, attracting the interest of many researchers.

This paper presents a new upper bound formulation using rigid finite elements and nonlinear programming and applies the formulation to slope stability problems in two and three dimensions (2D or 3D). Rigid finite elements are employed to discretize the slope media. A velocity discontinuity may occur at any edge or face that is shared by adjacent elements. To ensure that the computed velocity field is kinematically admissible, the unknowns are subject to linear and nonlinear equality constraints as well as linear inequality constraints that are generated by an energy–work balance equation, the Mohr–Coulomb failure criterion, an associate flow rule, and the boundary conditions. This leads to a standard nonlinear optimization problem. The objective function of the problem is to find the minimum value of the factor of safety using an optimization method. In this paper, the solution to this optimization problem is obtained by using a sequential quadratic algorithm.

Numerical formulation of upper bound theorem based on rigid finite elements

Rigid finite element discretization

The discretization of the soil media in a slope using the rigid finite element (RFE) is similar to that in the case of the conventional finite element (FE) method, except that the RFEM assumes all elements are rigid. The slope is divided into a proper number of rigid elements mutually connected at the interfaces. In such a discrete model, displacements (or velocities) of any point in a rigid element can be described as a function of the translation and rotation of the element centroid. The deformation energy of the system is stored only in the interfaces of all elements. The displacement of an interface, which is the embodiment of relative displacement of adjacent rigid elements, shows a discontinuous feature. It should be pointed out that, despite the discontinuous feature at the interfaces, the studied media can still be considered to be a continuum as a whole mass body.

In our numerical implementation of the upper bound theorem for slope stability analysis, the soil mass is first discretized into a number of simple rigid finite elements, namely, triangular elements in a 2D case or tetrahedral elements in a 3D case. Kinematically admissible velocity discontinuities are permitted at all interfaces shared by adjacent elements. If D is the dimensionality of a problem (where D is equal to 2 for a 2D or 3 for a 3D case) then each element

is associated with $D(D + 1)/2$ dimensional vector $\boldsymbol{V}_g$ of velocity variables at its centroid, i.e., $\boldsymbol{V}_g = \{v_i\}^T$ where $i = 1,...,D(D + 1)/2$, and T denotes transpose.

Lyamin and Sloan (2002) used velocities at the node points to define the displacement of an element. Our approach of using the velocity at the centroid is simpler. With this approach, the velocity vector $\boldsymbol{V}(x, y, z)$ at any point $p(x, y, z)$ within an element can be completely expressed in terms of the $\boldsymbol{V}_g$ at the corresponding centroid of the element, as given in eq. [1]

$$[1] \qquad \boldsymbol{V}(x, y, z) = \boldsymbol{N}\boldsymbol{V}_g$$

where $\boldsymbol{N}$ is the shape function. In the 2D case

$$[2] \qquad \boldsymbol{N} = \begin{bmatrix} 1 & 0 & -(y - y_g) \\ 0 & 1 & (x - x_g) \end{bmatrix}$$

and in the 3D case

$$[3] \qquad \boldsymbol{N} = \begin{bmatrix} 1 & 0 & 0 & 0 & (z - z_g) & -(y - y_g) \\ 0 & 1 & 0 & -(z - z_g) & 0 & (x - x_g) \\ 0 & 0 & 1 & (y - y_g) & -(x - x_g) & 0 \end{bmatrix}$$

The global xyz coordinate system is shown in Fig. 1. For analysis of displacement and forces on a rigid element, it is more convenient to use a local reference coordinate system of n–d–s axes on one planar face of the element. In Fig. 1, the n-axis is along the outward normal of the face; the d-axis is the dip direction (the steepest descent on the face); and the s-axis is the strike direction (parallel to the projected intersection between the xy-plane and the face). The n–d–s axes form a right-handed coordinate system.

Figure 2 shows two tetrahedron elements (1) and (2) with global velocities $\boldsymbol{V}^{(1)}$ and $\boldsymbol{V}^{(2)}$, respectively, (magnitude denoted as $v^{(1)}$ and $v^{(2)}$) at point P in a 3D case. As shown in Fig. 2, point P on the interface of element (1) moves at velocity $\boldsymbol{V}^{(1)}_{local}$, and the same point P on the interface of element (2) moves at velocity $\boldsymbol{V}^{(2)}_{local}$. The two velocities $\boldsymbol{V}^{(1)}_{local}$ and $\boldsymbol{V}^{(2)}_{local}$ take the same local coordinate axes at the interface on element (1) as the reference system. The relative velocity jump can be expressed as $\Delta\boldsymbol{V}^{(2-1)}_{local} = \boldsymbol{V}^{(2)}_{local} - \boldsymbol{V}^{(1)}_{local}$. Using the local n–d–s coordinate system, components of velocity $\boldsymbol{V}^{(1)}_{local}$ and $\boldsymbol{V}^{(2)}_{local}$ in the normal, dip, and strike directions can be respectively expressed as $\boldsymbol{V}^{(1)}_n$, $\boldsymbol{V}^{(1)}_d$, $\boldsymbol{V}^{(1)}_s$ for element (1) and $\boldsymbol{V}^{(2)}_n$, $\boldsymbol{V}^{(2)}_d$, $\boldsymbol{V}^{(2)}_s$ for element (2). The relative velocity $\Delta\boldsymbol{V}^{(2-1)}_{local}$ at point P can be decomposed into three components: normal direction by $\Delta\boldsymbol{V}^{(2-1)}_n$, dip direction by $\Delta\boldsymbol{V}^{(2-1)}_d$, and the strike direction by $\Delta\boldsymbol{V}^{(2-1)}_s$, that is, $\Delta\boldsymbol{V}^{(2-1)}_{local} = [\Delta\boldsymbol{V}^{(2-1)}_n, \Delta\boldsymbol{V}^{(2-1)}_d, \Delta\boldsymbol{V}^{(2-1)}_s]^T$.

The relative velocity jump at point P can be written as

$$[4] \qquad \Delta\boldsymbol{V}^{(2-1)}_{local} = (\boldsymbol{V}^{(2)}_{local} - \boldsymbol{V}^{(1)}_{local}) = [(\boldsymbol{V}^{(2)}_n - \boldsymbol{V}^{(1)}_n), (\boldsymbol{V}^{(2)}_d - \boldsymbol{V}^{(1)}_d), (\boldsymbol{V}^{(2)}_s - \boldsymbol{V}^{(1)}_s)]^T$$

For convenience, we denote $\Delta\boldsymbol{V}^{(2-1)}_{local}$ as $\Delta\boldsymbol{V}$ in the rest of paper. The above velocity jump expressed in terms of the velocities in the local coordinate system can be expressed by the velocities $\boldsymbol{V}^{(1)}$ and $\boldsymbol{V}^{(2)}$ in the global coordinate system

$$[5] \qquad \Delta\boldsymbol{V} = (\boldsymbol{V}^{(2)}_{local} - \boldsymbol{V}^{(1)}_{local}) = (\boldsymbol{L}^{(1)}\boldsymbol{V}^{(2)} - \boldsymbol{L}^{(1)}\boldsymbol{V}^{(1)})$$

where $\boldsymbol{L}^{(1)}$ is the matrix of direction cosines of the local n–d–s axes on the interface of element (1) with respect to the global coordinate system and is expressed by

$$[6] \qquad \boldsymbol{L}^{(1)} = \begin{bmatrix} \cos(\boldsymbol{n}, \boldsymbol{x}) & \cos(\boldsymbol{n}, \boldsymbol{y}) & \cos(\boldsymbol{n}, \boldsymbol{z}) \\ \cos(\boldsymbol{d}, \boldsymbol{x}) & \cos(\boldsymbol{d}, \boldsymbol{y}) & \cos(\boldsymbol{d}, \boldsymbol{z}) \\ \cos(\boldsymbol{s}, \boldsymbol{x}) & \cos(\boldsymbol{s}, \boldsymbol{y}) & \cos(\boldsymbol{s}, \boldsymbol{z}) \end{bmatrix}$$

Using eq. [1] for the global velocity $\boldsymbol{V}_g$ at the element centroid, eq. [5] can be written as

$$[7] \qquad \Delta\boldsymbol{V} = \boldsymbol{L}^{(1)}[\boldsymbol{N}^{(2)}\boldsymbol{V}^{(2)}_g - \boldsymbol{N}^{(1)}\boldsymbol{V}^{(1)}_g]$$

Equation [7] can be given in the form

$$[8] \qquad \Delta\boldsymbol{V} = \boldsymbol{A}\boldsymbol{V}_G$$

where

$$\boldsymbol{A} = [\boldsymbol{L}^{(1)} - \boldsymbol{L}^{(1)}] \begin{bmatrix} \boldsymbol{N}^{(2)} & 0 \\ 0 & \boldsymbol{N}^{(1)} \end{bmatrix}$$

and

$$\boldsymbol{V}_G = \begin{Bmatrix} \boldsymbol{V}^{(2)}_g \\ \boldsymbol{V}^{(1)}_g \end{Bmatrix}$$

Constraints in velocity discontinuities

Soil fails when the maximum shear stress reaches its shear strength. The shear strength can usually be described by the Mohr–Coulomb failure (or yield) criterion

$$[9] \qquad |\tau| = c' + \sigma'_n \tan\phi'$$

where τ and σ'_n are the shear stress and the effective normal stress at failure, respectively, and c' and ϕ' are the effective cohesion and friction angle, respectively. It is noted that the effective normal stress $\sigma'_n = \sigma_n - u$, where σ_n and u are the total normal stress and the pore-water pressure, respectively.

Velocity discontinuities are allowed to occur at any edge or face that is shared by a pair of adjacent triangles or tetrahedrons. To be kinematically admissible, the velocity discontinuities must satisfy a plastic flow rule. According to the Mohr–Coulomb failure (or yield) criterion and the associated flow rule, the relationship between the normal velocity magnitude (Δv_n) and tangential velocity magnitude (Δv_t) jumps across the discontinuity can be written as

$$[10] \qquad \Delta v_n = |\Delta v_t| \tan\phi'$$

The existence of the absolute value sign on the right hand side of eq. [10] makes it difficult to derive a set of flow rule constraints that are everywhere differentiable. It is clear that Δv_t may be zero, negative, or positive. From the mathematical programming point of view, this is referred to as an unrestricted-in-sign variable. Any unrestricted quantity can be decomposed into the difference of two non-negative quantities. Thus, the tangential velocity jump $\Delta\boldsymbol{V}_t$ defined in the local n–d–s coordinate system can be decomposed into two sets of non-negative variables $\boldsymbol{V}^+$ and $\boldsymbol{V}^-$

$$[11] \qquad \Delta\boldsymbol{V}_t = \boldsymbol{V}^+ - \boldsymbol{V}^-$$

Fig. 1. Local coordinate system defined by *n* (normal direction), *d* (dip direction), and *s* (strike direction).

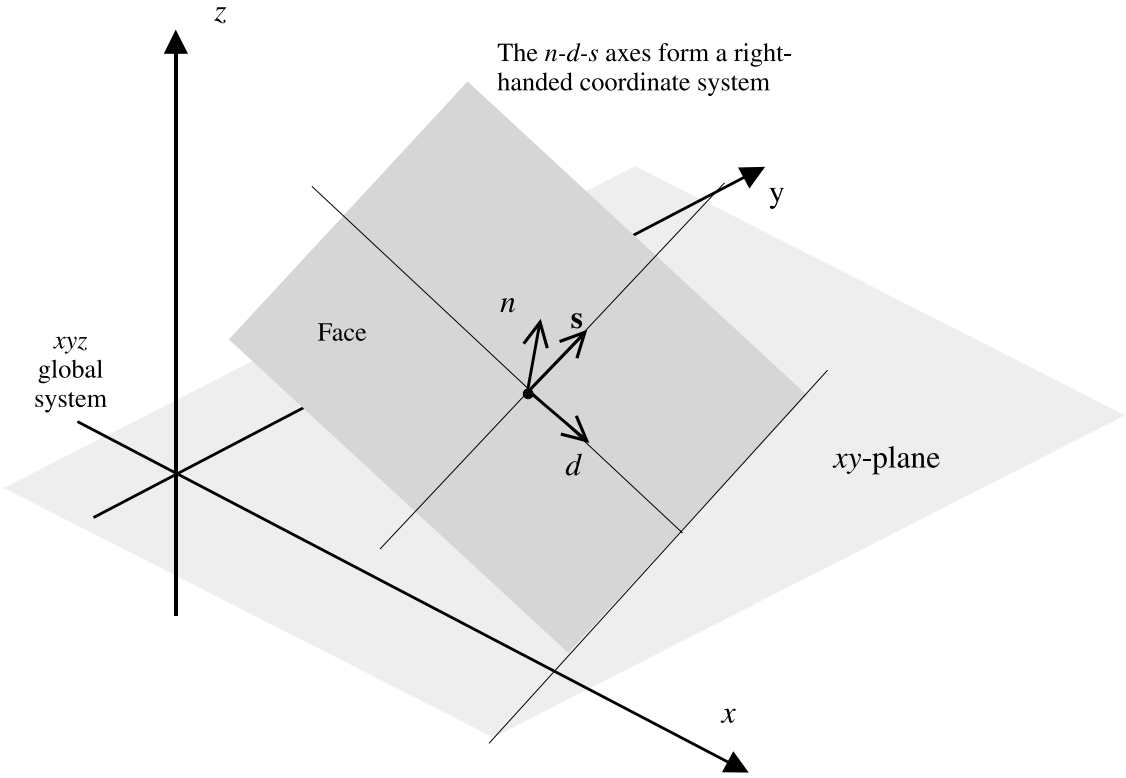

Fig. 2. Three-dimensional velocity discontinuity.

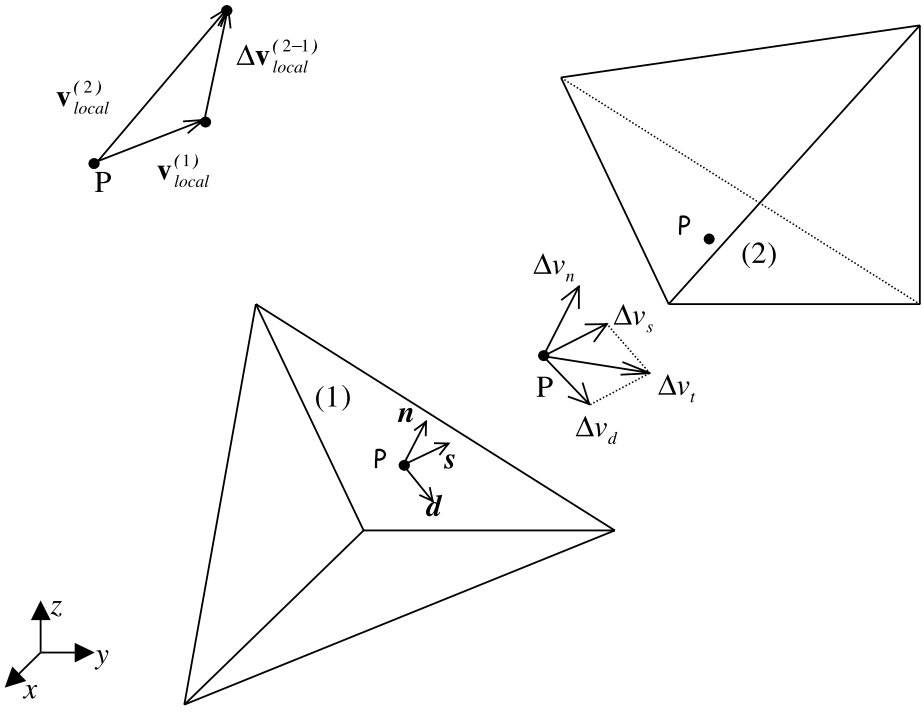

where

$$\Delta \boldsymbol{V}_t = \{\Delta v_d, \Delta v_s\}^T$$

$$\boldsymbol{V}^+ = \{v_1^+, \ldots, v_{D-1}^+\}^T$$

$$\boldsymbol{V}^- = \{v_1^-, \ldots, v_{D-1}^-\}^T$$

with the constraints

$$[12] \quad \begin{matrix} v_i^+ \geq 0 \\ v_i^- \geq 0 \end{matrix} \qquad (i = 1, \ldots, D-1)$$

To remove the absolute value sign, and thus set the equation into a standard mathematic programming problem, we follow the formulation derived by Sloan and Kleeman (1995) and Lyamin and Sloan (2002). Hence $\left|\Delta v_t\right|$ is given by

$$[13] \quad \left|\Delta v_t\right| \leq \sum_{i=1}^{D-1} (v_i^+ + v_i^-)$$

Therefore, the tangential velocity jump is automatically determined by finding the values of D–1 pairs of unknown variables v_i^+ and v_i^-, without any sign restrictions. The normal velocity jump is given by

$$[14] \quad \left|\Delta v_n\right| \leq \sum_{i=1}^{D-1} (v_i^+ + v_i^-) \tan\phi'$$

Using the same simplification as that used by Sloan and Kleeman (1995) and Lyamin and Sloan (2002), the formulation in eq. [13] in this paper is taken as

$$[15] \quad \left|\Delta v_t\right| = \sum_{i=1}^{D-1} (v_i^+ + v_i^-)$$

Thus, in matrix notation, conditions from eqs. [11]–[15] can be written as

$$[16] \quad \begin{matrix} \Delta \boldsymbol{V} = \boldsymbol{B}\boldsymbol{V}_d \\ \boldsymbol{V}_d \geq 0 \end{matrix}$$

where

$$\boldsymbol{V}_d = \{v_1^+, v_1^-, \ldots, v_{D-1}^+, v_{D-1}^-\}^T$$

in the 2D case

$$\boldsymbol{B} = \begin{bmatrix} \tan\phi' & \tan\phi' \\ 1 & -1 \end{bmatrix}$$

and in the 3D case

$$\boldsymbol{B} = \begin{bmatrix} \tan\phi' & \tan\phi' & \tan\phi' & \tan\phi' \\ 1 & -1 & 0 & 0 \\ 0 & 0 & 1 & -1 \end{bmatrix}$$

Boundary conditions

As stated in the upper bound theorem, the velocity field must satisfy the prescribed velocity boundary conditions. Considering element k on a boundary where the prescribed velocity is $\bar{\boldsymbol{V}}$, the element velocity $\boldsymbol{V}_g^k$ must satisfy the following equality

$$[17] \quad \boldsymbol{V}_g^k = \bar{\boldsymbol{V}}$$

Equivalent load

Because we set the velocities at all element centroids as unknown variables in the RFEM, correspondingly the external force must be first converted into an equivalent load of the element centroid. It is possible to simplify the calculation of such an equivalent load by using the natural coordinate system, which relies on the element geometry and whose coordinates range between zero and unity within the element. A 2D natural coordinate system is shown in Fig. 3.

We define the natural coordinates as $L_i = A_i/A$ (i = 1, 2, 3) in a plane problem where A_i (i = 1, 2, 3) are the areas of sub-triangles 0–2–3, 0–3–1, and 0–1–2, and A is the total area of triangle 1–2–3.

The natural coordinates in two dimensions have the following features:

$$[18] \quad \begin{matrix} \sum_{i=1}^{3} L_i = 1 \\ \sum_{i=1}^{3} L_i x_i = x \\ \sum_{i=1}^{3} L_i y_i = y \end{matrix}$$

$$[19] \quad \iint_A L_1^a L_2^b L_3^c \, dx\, dy = \frac{a!\,b!\,c!}{(a+b+c+2)!} 2A$$

Mechanical loads consist of surface traction and body force. In geotechnical applications gravity is a common form of body force that can be applied directly to a RFEM modal, while surface traction must be converted to an equivalent centroid load $\boldsymbol{Q}$.

Figure 4 shows a uniformly distributed traction in a 2D case in the negative y direction, $\boldsymbol{q} = [0 \; -q]^T$. The calculation of its equivalent load would involve the features of the 1D natural coordinate system, such as

$$[20] \quad \begin{matrix} x = L_1 x_1 + L_2 x_2 \\ y = L_1 y_1 + L_2 y_2 \\ \int_L L_1^a L_2^b \, dl = \frac{a!\,b!}{(a+b+1)!} L \end{matrix}$$

Its equivalent load $\boldsymbol{Q}$ at the centroid of the element can be calculated as the following:

$$[21] \quad \begin{aligned} \boldsymbol{Q} &= \int_{l_{AB}} \boldsymbol{N}^T \boldsymbol{q} \, dl \\ &= \int_{l_{AB}} \begin{bmatrix} 1 & 0 & y_g - y \\ 0 & 1 & x - x_g \end{bmatrix}^T \begin{Bmatrix} 0 \\ -q \end{Bmatrix} dl \\ &= \int_{l_{AB}} [0 \quad -q \quad (x_g - x)\, q]^T dl \\ &= \begin{bmatrix} 0 & \int_{l_{AB}} -q \, dl & \int_{l_{AB}} q x_g \, dl - \int_{l_{AB}} q (L_1 x_1 + L_2 x_2) \, dl \end{bmatrix}^T \end{aligned}$$

Substituting eq. [20] into eq. [21], we can get

$$[22] \quad \boldsymbol{Q} = [0 \quad -q l_{AB} \quad q l_{AB} (x_g - x_c)]^T$$

where l_{AB} is the length of the edge AB, and x_c is the abscissa at the centre of the edge AB.

Note that the equivalent centroid load of pore-water force $\boldsymbol{P}$ can be obtained similarly according to the formulations discussed above. The development of natural coordinates

Fig. 3. Natural coordinates.

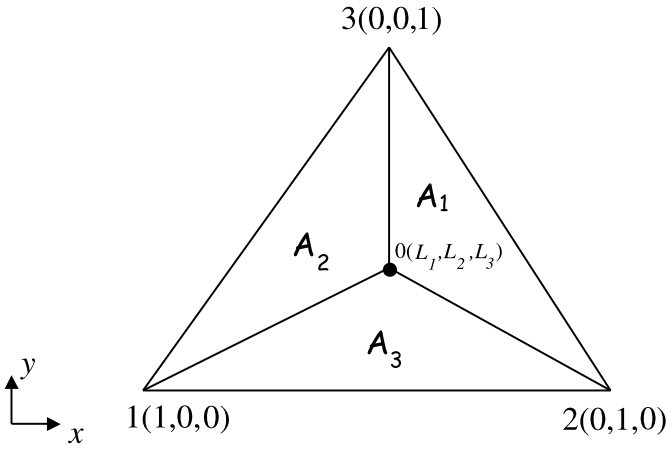

and the calculation of equivalent load for tetrahedron elements follow the same procedure used for the 2D case.

Energy–work balance equation

According to the virtual work principle, the total internal power dissipation is equal to the total work done by external forces

$$[23] \quad \int_{\Omega^*} \sigma'_{ij}\ \dot{\varepsilon}^*_{ij}\,\mathrm{d}\Omega^* + \int_{\Gamma^*} \sigma'_{\Gamma'}\ \dot{\varepsilon}^*_{\Gamma^*}\,\mathrm{d}\Gamma^* = \boldsymbol{W}\,\boldsymbol{V}^* + \boldsymbol{Q}\boldsymbol{V}^* + \boldsymbol{P}\boldsymbol{V}^*$$

Equation [23] is an energy–work balance equation. The first term on the left-hand side of eq. [23] is the rate of work done by the effective stress σ'_{ij} over the virtual strain rates $\dot{\varepsilon}^*_{ij}$, dissipated within Ω^*. The second left-hand side term is the internal energy dissipation along the slip surface and discontinuities Γ^*. The right-hand side terms in eq. [23] represent the rate of external work done by the weight of the sliding mass $\boldsymbol{W}$, the surface equivalent loads $\boldsymbol{Q}$, and the equivalent pore-water force $\boldsymbol{P}$ over the virtual plastic velocity $\boldsymbol{V}^*$.

According to the rigid assumption for the elements, there is no energy dissipation within elements. Thus, the first term on the left-hand side of eq. [23] equals zero, that is, $\int_{\Omega^*} \sigma'_{ij}\ \dot{\varepsilon}^*_{ij}\,\mathrm{d}\Omega^* = 0$. The power is dissipated only along the failure surface and the interfaces between the elements. The energy dissipated along the failure surface and the interfaces by normal and tangential stresses can be expressed by the following equation:

$$[24] \quad \int_{\Gamma^*} \sigma'_{\Gamma'}\ \dot{\varepsilon}^*_{\Gamma^*}\,\mathrm{d}\Gamma^* = \int_{S_\mathrm{d}} (|\tau \Delta v_\mathrm{t}| + \sigma'_\mathrm{n}\ \Delta v_\mathrm{n})\,\mathrm{d}S$$

Using the Mohr–Coulomb failure (or yield) criterion in eq. [9] and the associate flow rule in eq. [10], the right-hand side in eq. [24] can be written as

$$[25] \quad \int_{S_\mathrm{d}} (|\tau \Delta v_\mathrm{t}| + \sigma'_\mathrm{n}\ \Delta v_\mathrm{n})\,\mathrm{d}S = \int_{S_\mathrm{d}} c' |\Delta v_\mathrm{t}|\,\mathrm{d}S = \int_{S_\mathrm{d}} c' \left[\sum_{i=1}^{D\text{-}1} (v_i^+ + v_i^-)\right] \mathrm{d}S$$

Fig. 4. Uniformly distributed load on a triangle edge.

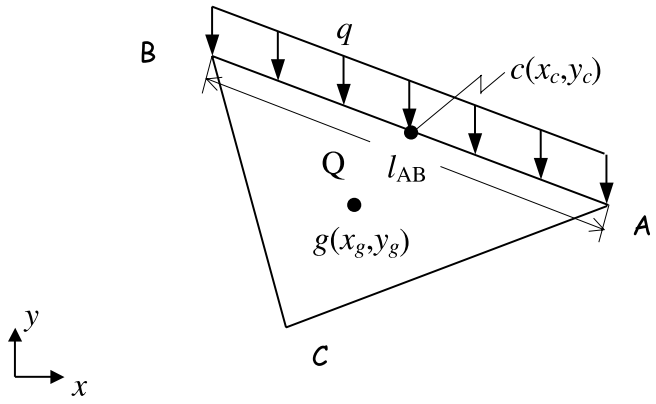

Note that eq. [25] does not include any stress. As a result, eq. [24] has no stress involvement in the calculation of the energy dissipation.

Using eq. [25], we can get

$$[26] \quad \int_{S_\mathrm{d}} c' \left[\sum_{i=1}^{D\text{-}1} (v_i^+ + v_i^-)\right] \mathrm{d}S = \boldsymbol{W}\,\boldsymbol{V}^*_\mathbf{g} + \boldsymbol{Q}\,\boldsymbol{V}^*_\mathbf{g} + \boldsymbol{P}\,\boldsymbol{V}^*_\mathbf{g}$$

Since all external forces $\boldsymbol{W}$, $\boldsymbol{Q}$, and $\boldsymbol{P}$ have been transferred to the centroid of the rigid element, the virtual velocity at the centroid $\boldsymbol{V}_\mathrm{g}$* shall be used. Assuming that the effective cohesion c' is identical at the discontinuity, eq. [26] can be written in the following general matrix form:

$$[27] \quad \boldsymbol{C}\boldsymbol{V}_\mathrm{d} = \boldsymbol{D}\boldsymbol{V}_\mathrm{g}$$

where $\boldsymbol{C} = \{c'_i l_i\}^\mathrm{T}$ for $i = 1,\ldots, n_\mathrm{D}$; $\boldsymbol{D} = \boldsymbol{W} + \boldsymbol{Q} + \boldsymbol{P}$; l_i is the length (in the 2D case) or the area (in the 3D case) of discontinuity i shared by two adjacent elements; and n_D is the total number of discontinuities.

Objective function

The stability of a slope is generally assessed by determining the factor of safety, F, by which the available shear strength parameters c' and ϕ' need to be reduced to bring the slope to a limit state of equilibrium. This definition of F is exactly the same as that used in limit equilibrium methods. The reduced parameters c'_e and ϕ'_e can therefore be defined by

$$[28] \quad c'_\mathrm{e} = \frac{c'}{F} \qquad \tan\phi'_\mathrm{e} = \frac{\tan\phi'}{F}$$

It thus renders a nonlinear programming problem while taking the reduced parameters c'_e and ϕ'_e into constraints given by the flow rule and the virtual work equation.

The classical upper bound theorem of limit analysis states that the loads determined by equating the external rate of work to the internal rate of plastic energy dissipation of a kinematically admissible velocity field are not less than the actual collapse load. For slope stability analysis, the factor of safety determined by the virtual work equation is greater than or equal to the true solution. Thus, according to nonlinear programming, the upper bound limit analysis for slope

stability can be reduced to a minimization problem and the objective function is the minimization of the factor of safety.

Assembly of constraint equations

All of the steps that are necessary to formulate the upper bound theorem as an optimization problem have now been covered. Note here that the reduced parameters have been taken into account in the constraints, i.e., the nonlinear form of the unknown variable F would appear in the constraints.

The task of finding a kinematically admissible velocity field that minimizes the factor of safety may be stated as

Minimize F subject to

$$[29]\quad \begin{cases} \Delta \boldsymbol{V} = \boldsymbol{A}\boldsymbol{V}_{\mathrm{G}} \\ \Delta \boldsymbol{V} = \boldsymbol{B}\boldsymbol{V}_{\mathrm{d}} \\ \boldsymbol{C}\boldsymbol{V}_{\mathrm{d}} = \boldsymbol{D}\boldsymbol{V}_{\mathrm{g}} \\ \boldsymbol{V}_g^k = \overline{\boldsymbol{V}} \\ \boldsymbol{V}_d \geq 0 \end{cases}$$

where

$$\boldsymbol{B} = \begin{bmatrix} \tan\phi_{\mathrm{e}}' & \tan\phi_{\mathrm{e}}' & \tan\phi_{\mathrm{e}}' & \tan\phi_{\mathrm{e}}' \\ 1 & -1 & 0 & 0 \\ 0 & 0 & 1 & -1 \end{bmatrix}$$

$$\boldsymbol{C} = \{c_{ie}'\ l_i\}^{\mathrm{T}} \qquad i = 1,\ldots,n_D$$

In two dimensions, each triangular element has three unknown velocities, and each velocity discontinuity has two unknown non-negative variables. In the 3D case, each tetrahedral element has six unknown velocities, and each planar interelement discontinuity has four unknowns. After imposing the flow rule conditions in the discontinuities, the velocity boundary conditions, and virtual work equation constraint, the unknowns must satisfy a set of equalities and inequalities. The objective function and the inequality constraints are linear, while because of the appearance of the nonlinear form of the unknown variable F, the equality constraints could be separated into linear and nonlinear equalities.

Optimization

The numerical formulation of the upper bound theorem presented in the previous sections results in an optimization problem that belongs to the class of nonlinear programming. The standard optimization theory (Jorge and Stephen 1999) indicates that the sequential quadratic programming (SQP) approach is one of the most effective methods for solving such a problem. In this study, we utilize the optimization toolbox in MATLAB (e.g., Penny 2000) to implement the SQP algorithm to find the minimum factor of safety of slopes.

Test examples

Based on the method discussed above, a computer program UBRFEM has been coded for 2D and 3D slope stability analyses. Four typical test problems that have been documented in the literature are analysed to investigate the feasibility of the present method.

Fig. 5. A weightless slope with a vertical surface load (Sokolovski 1960) — example 1.

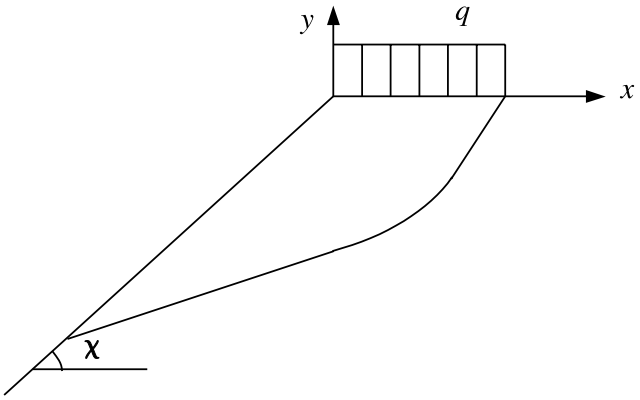

Strip pressure loading on the crest of a 2D slope — example 1

We first consider an example in two dimensions that has been documented in Sokolovski's (1960) book. As shown in Fig. 5, a vertical surface load is applied on a uniform, weightless slope with the following shear strength parameters: cohesion c equal to 98 kPa, friction angle ϕ equal to 30°, and the inclination of the slope χ equal to 45°. For this example, results are presented for three different meshes that are classified as coarse, medium, and fine, as illustrated in Fig. 6. The resultant factors of safety are listed in Table 1.

The slip-line analysis results in a closed-form solution with the ultimate load q equal to 111.44 kPa. Associated with this load, Chen (1999) used the upper bound theorem, which is based on the energy–work balance equation, and thus obtained a failure mode that gave the minimum value of F = 1.006. For the coarsest mesh shown in Fig. 6*a*, we obtain F = 1.034, while for the medium mesh illustrated in Fig. 6*b*, we obtain a value of F = 1.012. The best result is obtained using the fine mesh shown in Fig. 6*c*, that is, F = 1.003, which is very close to the theoretical solution, and is better than the solution obtained by Chen (1999).

The results for the three different meshes demonstrate that the solutions based on the proposed method are dependent on the mesh size. The finer the mesh, the better the results. However, it should be pointed out that the solution time and cost could dramatically increase with mesh refinement.

A symmetrical wedge — example 2

Figure 7 shows a 3D example of a specific symmetrical wedge with geometric values and strength parameters listed in Table 2. The mesh used to analyse this problem is shown in Fig. 8. For a given value of cohesion (varies from 5 to 20 kPa), the friction angle varies from 15 to 30°, and the factors of safety determined by the general limit equilibrium method (GLE) for a dilation angle equal to the friction angle ($\psi = \phi$), an upper bound method (Wang 2001), and the present approach are tabulated in Table 3. It shall be noted that the upper bound method (Wang 2001) uses the inclined slices and gives an upper bound value for the factor of safety. It has been shown that the GLE with $\psi = \phi$ (full dila-

Table 1. Results of factor of safety — example 1.

Theory	Upper bound (Chen 1999)	Present method (coarse mesh)	Present method (medium mesh)	Present method (fine mesh)
1.000	1.006	1.034	1.012	1.003

Fig. 6. The RFEM meshes of example 1 — (*a*) coarse mesh, (*b*) medium mesh, and (*c*) fine mesh.

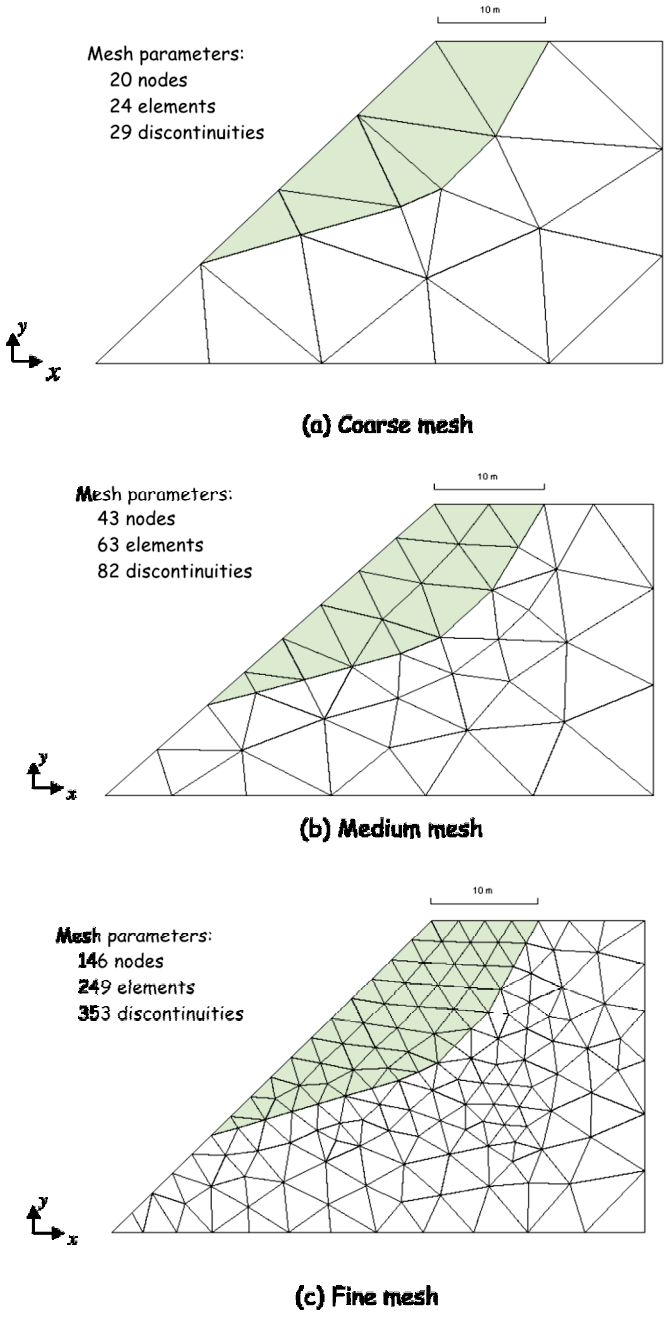

tion) gives an F value close to the upper bound value. From the comparison in Table 3, the results of the present method are close to those obtained by using the GLE method (Wang and Yin 2002) and the upper bound method (Wang 2001). It is also seen in Table 3 that the factor of safety increases with an increase in the friction angle for a given value of cohesion, or increases with the cohesion for a given friction angle. The comparison in Table 3 shows that the present method gives reasonable upper bound values of the factor of safety for the wedge problem studied.

Fig. 7. A symmetrical wedge in geometry — example 2.

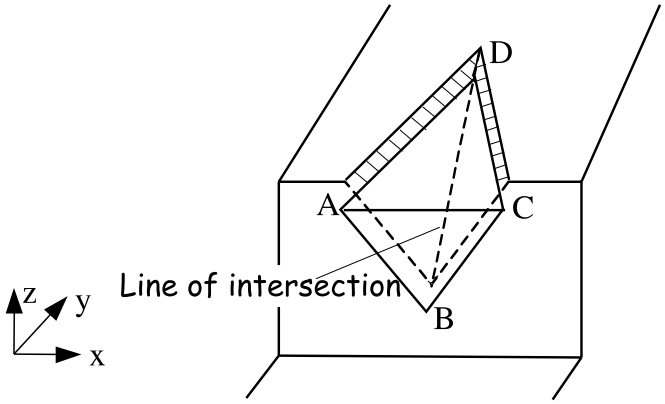

Table 2. Geometry and unit weight for a symmetrical wedge — example 2.

	Dip direction (°)	Dip (°)
Left discontinuity surface	120	65
Right discontinuity surface	240	65
Top surface	180	0
Slope surface	180	90

Note: γ = 26.46 kN/m^3, H = 10.2 m.

A nonsymmetrical wedge — example 3

The third example is a nonsymmetrical wedge that is frequently quoted in the literature (Hoek and Bray 1977), as shown in Fig. 9. The discretization pattern of this wedge is similar to that in example 2. The geometric and material properties of the wedge are listed in Table 4. The resulting factors of safety are presented in Table 5. For this example, the F value for the conventional limit equilibrium method (TLE) (e.g., Hoek and Bray 1977; Wang 2001) is 1.846, and the same result of 1.929 is obtained by both the GLE method for $\psi = \phi$ (full dilation) and the upper bound method (Wang 2001).

It shall be pointed out that the TLE method assumes that the two shear resistance forces on the two discontinuous planes of the wedges are parallel to the direction of the intersection of the two discontinuous planes, and this implies zero dilation of the two discontinuous planes (or joints). The GLE method with $\psi = \phi$ and the upper bound method (Wang 2001) assume full dilation of the two discontinuous planes. The present method also assumes full dilation. Therefore, it is more meaningful to compare the present method with the GLE method and the upper bound method (Wang 2001).

Fig. 8. The RFEM discretization — example 2.

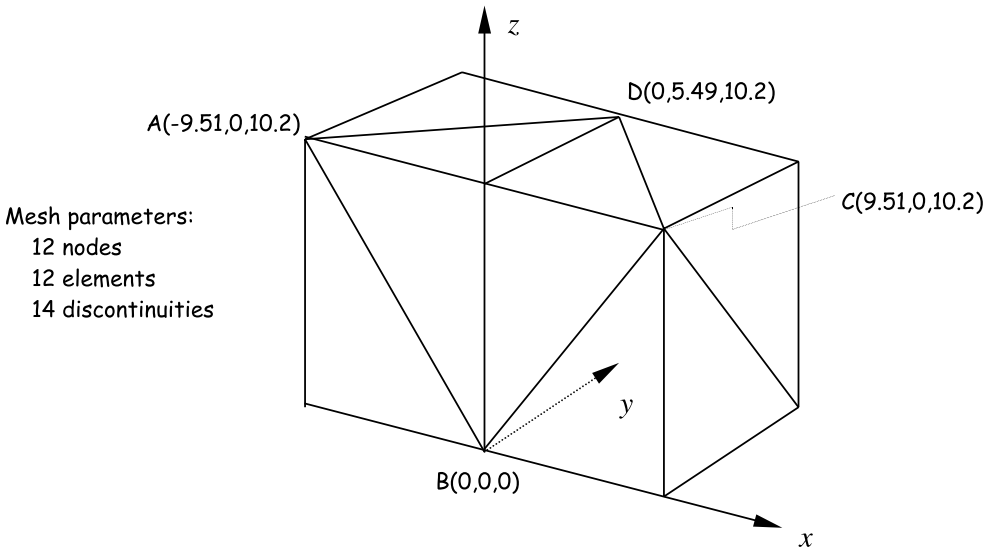

Table 3. Results of the factor of safety for a symmetrical wedge — example 2.

c (kPa)	Method	$\phi = 15$	$\phi = 30$
5	GLE (Wang and Yin 2002) ($\psi = \phi$)	0.675	1.279
	Upper bound (Wang 2001)	0.675	1.278
	Present method	0.668	1.272
15	GLE (Wang and Yin 2002) ($\psi = \phi$)	0.835	1.430
	Upper bound (Wang 2001)	0.835	1.430
	Present method	0.845	1.433
20	GLE (Wang and Yin 2002) ($\psi = \phi$)	1.173	1.749
	Upper bound (Wang 2001)	1.173	1.749
	Present method	1.173	1.755

Using the present approach, the factor of safety minimized by using a sequential quadratic algorithm is 1.937. The relative difference between the present solution and the two solutions obtained by the GLE method and the upper bound method is only 0.4%.

A spherical purely cohesive slope — example 4

Figure 10 shows a simple 3D problem of a uniform purely cohesive soil slope with a spherical slip surface (Lam and Fredlund 1993). The plan view of its discretization pattern is illustrated in Fig. 11. The present method gives a solution of $F = 1.436$, which is a little higher than the so-called "closed-form" solution of $F = 1.402$, reported by Lam and Fredlund (1993). The relative difference is 2.4%.

Conclusions

A new upper bound method for the analysis of two- and three-dimensional slope stability problems is presented in this paper. Based on the rigid finite elements, the stability problem is formulated as a nonlinear programming optimization problem. The factor of safety of a slope is optimized (minimized) using a sequential quadratic programming algorithm.

Fig. 9. A nonsymmetrical wedge (Hoke and Bray 1977) — example 3.

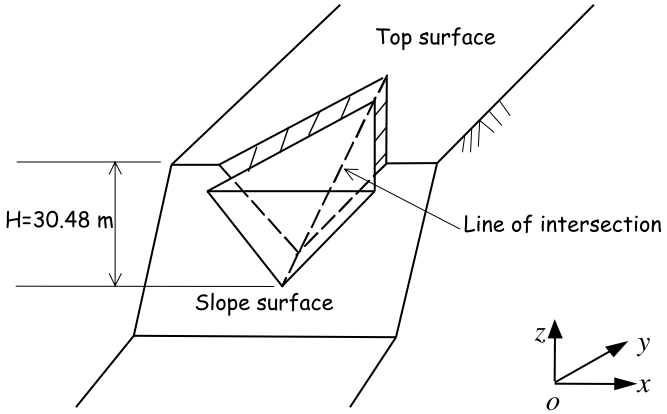

The validation of the proposed method and the associated program has been demonstrated through four typical examples. Results obtained using the present method are in agreement with those obtained using other commonly used methods. The proposed method is simpler than a similar method employing linear finite elements used by Sloan (1988, 1989), Sloan and Kleeman (1995), and Lyamin and Sloan (2002). The proposed method is superior to the upper bound method by Donald and Chen (1997) in modelling nonhomogenous soil conditions and complicated boundary conditions.

Acknowledgements

The research work presented and the preparation of the paper have received financial support from a RGC (Research Grants Council) grant (PolyU 5064/00E) of the University Grants Committee (UGC) of the Hong Kong SAR Government of China and the Hong Kong Polytechnic University. These financial supports are gratefully acknowledged. The authors are grateful to Professor Zuyu Chen and Professor Dave Chan for their technical advice on the research project.

Fig. 10. A spherical slip surface in a purely cohesive soil — example 4.

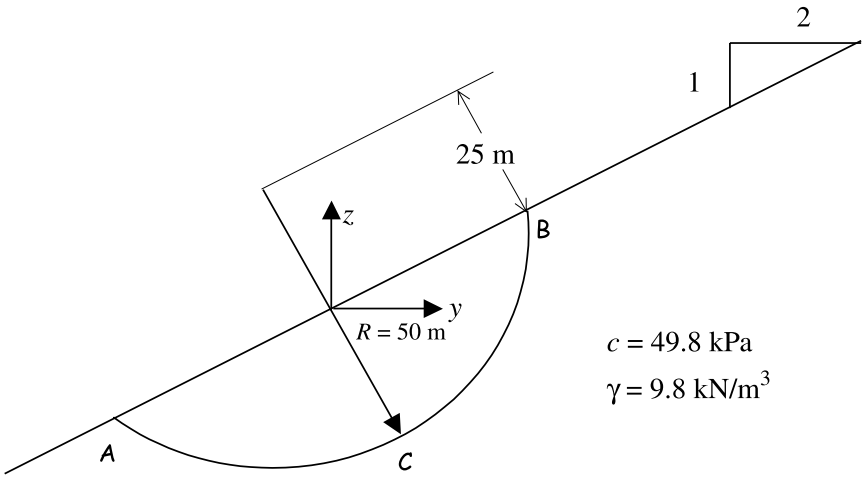

Table 4. Wedge geometry and material strength parameters — example 3.

Plane	Dip direction (°)	Dip (°)	Properties and slope height
Discontinuity 1	105	45	c_1 = 23.9 kN/m^2 (500 lb/ft^2), ϕ = 20°
Discontinuity 2	235	70	c_2 = 47.9 kN/m^2 (1000 lb/ft^2), ϕ = 30°
Slope surface	185	65	γ = 25.2 kN/m^3 (160 lb/ft^3)
			γ_w = 9.81 kN/m^3 (62.5 lb/ft^3)
Top surface	195	12	H = 30.48 m (100 ft)

Note: After Hoek and Bray (1977) and water pressure not considered.

Table 5. Results of factor of safety — example 3.

TLE (Hoek and Bray 1977; Wang 2001)	GLE ($\psi = \phi$) (Wang and Yin 2002)	Upper bound (Wang 2001)	Present method
1.846	1.929	1.929	1.937

Fig. 11. A plan view of the discretization pattern — example 4.

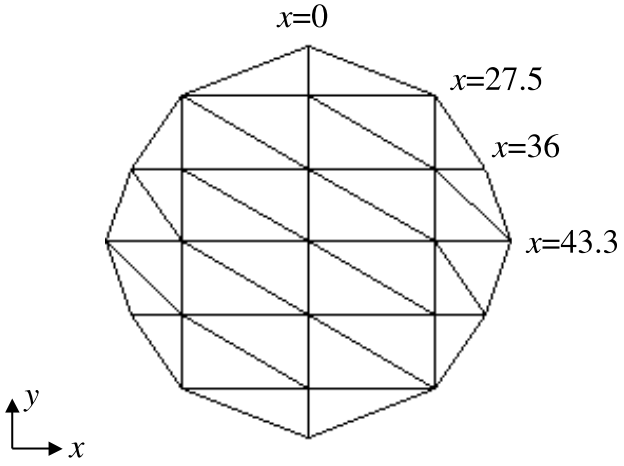

Table 6. Results of factor of safety — example 4.

Close-form (Lam and Fredlund 1993)	Present method
1.402	1.436

References

Bishop, A.W. 1955. The use of the slip circle in the stability analysis of slopes. Géotechnique, **5**: 7–17.

Chen, W.F. 1975. Limit analysis and soil plasticity. *In* Developments in geotechnical engineering No. 7. Elsevier Scientific Publishing Co., New York.

Chen, Z.Y. 1999. The limit analysis for slopes: Theory, methods and applications. *In* Proceedings of the International Symposium on Slope Stability Engineering. *Edited by* N. Yagi, T. Yamagami, and J.C. Jiang. Shikoku, pp. 15–29.

Chen, Z.Y., Wang, X.G., Haberfield, C., Yin, J.H., and Wang, Y.J. 2001*a*. A three-dimensional slope stability analysis method using the upper bound theorem Part I: theory and methods. International Journal of Rock Mechanics and Mining Sciences, **38**: 369–378.

Chen, Z.Y., Wang, J., Wang, Y.J., Yin, J.H., and Haberfield, C. 2001*b*. A three-dimensional slope stability analysis method using the upper bound theorem Part II: numerical approaches, applications and extensions. International Journal of Rock Mechanics and Mining Sciences, **38**: 379–397.

Donald, I.B., and Chen, Z. 1997. Slope stability analysis by the upper bound approach: fundamentals and methods. Canadian Geotechnical Journal, **34**: 853–862.

Drucker, D.C., and Prager, W. 1952. Soil mechanics and plastic analysis or limit design. Quarterly of Applied Mathematics, **10**: 157–165.

Griffths, D.V., and Lane, P.A. 1999. Slope stability analysis by finite elements. Géotechnique, **49**(3): 387–403.

Hoek, E. 1987. General two-dimensional slope stability analysis. *In* Analytical and computational methods in engineering rock mechanics. *Edited by* E.T. Brown. Allen & Unwin, London, pp. 95–128.

Hoek, E., and Bray, J.W. 1977. Rock slope engineering. The Institution of Mining and Metallurgy, London.

Janbu, N. 1973. Slope stability computations. *In* Proceedings of Embankment Dam Engineering. *Edited by* R.C. Hirschfield and J. Poulos. John Wiley & Sons, New York, pp. 47–86.

Jorge, N., and Stephen, J.W. 1999. Numerical optimization. Springer-Verlag Inc., New York.

Kawai, T. 1978. New discrete models and their application to seismic response analysis of structures. Nuclear Engineering Design, **48**: 207–229.

Kim, J., Salgado, R., and Yu, H.S. 1999. Limit analysis of soil slopes subjected to pore-water pressures. Journal of Geotechnical and Geoenvironmental Engineering, ASCE, **125**(1): 49–58.

Lam, L., and Fredlund, D.G. 1993. A general limit-equilibrium model for three-dimensional slope stability analysis. Canadian Geotechnical Journal, **30**: 905–913.

Lyamin, A.V., and Sloan, S.W. 2002. Upper bound limit analysis using linear finite elements and non-linear programming. International Journal for Numerical and Analytical Methods in Geomechanics, **26**: 181–216.

MacLaughlin, M., Sitar, N., Doolin, D., and Abbot, T. 2001. Investigation of slope-stability kinematics using discontinuous deformation analysis. International Journal of Rock Mechanics and Mining Sciences, **38**: 753–762.

Morgenstern, N.R., and Price, V.E. 1965. The analysis of stability of general slip surface. Géotechnique, **15**: 79–93.

Penny, J. 2000. Numerical methods using Matlab. Prentice Hall, Upper Saddle River, N.J.

Qian, L.X., and Zhang, X. 1995. Rigid finite element method and its applications in engineering. Acta Mechanica Sinica, **11**(1): 44–50.

Sarma, K.S. 1979. Stability analysis of embankments and slopes. Journal of Geotechnical Engineering, ASCE, **105**(12): 1511–1524.

Sloan, S.W. 1988. Lower bound limit analysis using finite elements and linear programming. International Journal for Numerical and Analytical Methods in Geomechanics, **12**: 61–77.

Sloan, S.W. 1989. Upper bound limit analysis using finite elements and linear programming. International Journal for Numerical and Analytical Methods in Geomechanics, **13**: 263–282.

Sloan, S.W., and Kleeman, P.W. 1995. Upper bound limit analysis using discontinuous velocity fields. Computer Methods in Applied Mechanics and Engineering, **127**: 293–314.

Sokolovski, V.V. 1960. Statics of soil media. *Translated by* D.H. Jones and A.N. Scholfield. Butterworth, London.

Wang, Y.J. 2001. Stability analysis of slopes and footings considering different dilation angles of geomaterial. Ph.D. thesis. Department of Civil and Structural Engineering, The Hong Kong Polytechnic University.

Wang, Y.J., and Yin, J.H. 2002. Wedge stability analysis considering dilatancy of discontinuities. Rock Mechanics and Rock Engineering, **35**(2): 127–137.

Wang, Y.J., Yin, J.H., and Lee, C.F. 2001. The influence of a non-associated flow rule on the calculation of the factor of safety of soil slopes. International Journal for Numerical and Analytical Methods in Geomechanics, **25**: 1351–1359.

Yu, H.S., Salgado, R., Sloan, S.W., and Kim, J.M. 1998. Limit analysis versus limit equilibrium for slope stability. Journal of Geotechnical and Geoenvironmental Engineering, ASCE, **124**(1): 1–11.

Zhang, X. 1999. Slope stability analysis based on the rigid finite element method. Géotechnique, **49**: 585–593.

Zhang, X., and Qian, L.X. 1993. Rigid finite element and limit analysis. Acta Mechanica Sinica, **9**(2): 156–162.

Zhang, J.H., Fan, J.W., and Hu, D. 1997. Theory and application of rigid body-spring element method. Chengdu Science and Technology Press, Cheng Du. [In Chinese.]

Zhang, J.H., He, J.D., and Fan, J.W. 2001. Static and dynamic stability assessment of slopes or dam foundations using a rigid body-spring element method. International Journal of Rock Mechanics and Mining Sciences, **38**: 1081–1090.